

Interplay between inelastic X-ray scattering and *ab initio* density-response calculations: Insight into the electronic correlations in aluminum

J. Z. Tischler¹, B. C. Larson^{*1}, P. Zschack², A. Fleszar³, and A. G. Egiluz⁴

¹ Condensed Matter Sciences Division, Oak Ridge National Laboratory, Oak Ridge, TN 37830, USA

² Materials Research Laboratory, University of Illinois, Urbana-Champaign Urbana, IL 61801, USA

³ Institut für Theoretische Physik, Universität Würzburg, Am Hubland, 97074 Würzburg, Germany

⁴ Department of Physics and Astronomy, University of Tennessee, Knoxville and Condensed Matter Sciences Division, Oak Ridge National Laboratory, Oak Ridge, TN 37831, USA

Received 25 October 2002, accepted 28 November 2002

Published online 30 April 2003

Dedicated to Professor Jozef T. Devreese on the occasion of his 65th birthday

PACS 71.15.Mb

Inelastic X-ray scattering (IXS) measurements on Al have been analyzed in conjunction with *ab initio*, time-dependent density functional theory (TDDFT) calculations of the electron–hole excitation spectrum. The dynamical structure factor evaluated with use of the many-body kernel f_{xc} obtained within the adiabatic extension of the local-density approximation (ALDA) is shown to be in good agreement with the IXS energy-loss data for energies up to about 20 eV, for momentum transfers up to twice the Fermi wave vector. For larger energy transfers the complex, frequency-dependent f_{xc} obtained by Devreese and collaborators via dynamical-exchange decoupling techniques is shown to lead to a description of the IXS data comparable with that of the ALDA. For low energies the ALDA works better, a conclusion with a simple physical interpretation. The analysis of the relative merits of the models for the many-body interactions is made using IXS cross sections that were obtained in absolute units; to this end, a procedure was introduced which is applicable for arbitrary materials, not just for *sp*-bonded Al.

1 Introduction Electron–electron interactions play a central role in determining the physical properties of materials, including all transport-related phenomena. Although short-range exchange-correlation effects have long been the subject of theoretical investigation [1–10], a full understanding of these effects, and their interplay with the band structure of real materials, remains a significant challenge. Inelastic X-ray scattering (IXS) measurements first addressed this area in 1967 [11]. However, it has taken the advent of 2nd and – especially – 3rd generation synchrotron sources, and high-resolution inelastic-scattering facilities, to open the detailed investigation [12–17] of the large wave-vector processes responsible for the short-range many-body effects. The experimental advances witnessed at synchrotrons have occurred concurrently with recent developments in *ab initio* electron density-response methods for periodic crystals (see, *e.g.*, the recent overviews in Refs. [18] and [19]). The exploitation of the direct linkage between density response and inelastic X-ray scattering through the dynamical structure factor $S(\mathbf{q}, \omega)$ as a function of wave vector \mathbf{q} and frequency ω represents a promising framework for the goal of a fundamental understanding of the electron correlations.

* Corresponding author: e-mail: bcl@ornl.gov

In this article we underscore the opportunity for meaningful insight into the dynamical correlations via a judicious interplay between time-dependent density-functional theory (TDDFT) [20] calculations of the electron-hole excitation spectrum in periodic crystals with state-of-the-art IXS measurements of $S(\mathbf{q}, \omega)$. As a test case, we consider the case of fcc Al. We show that the so-called many-body kernel f_{xc} obtained within the simple ansatz which corresponds to an adiabatic extension of the local-density approximation (ALDA) [20] provides a good overall description of exchange-correlation effects in Al up to about 20 eV, for wave vectors up to twice the Fermi wave vector. Making use of the availability of detailed frequency and wave vector dependent data [6], we also assess (by comparison with the IXS data) the performance of the explicit result for $f_{xc}(\omega)$ obtained by Devreese and collaborators [3, 6] via a dynamical-exchange decoupling method. We find the performance of this kernel to be comparable with the ALDA for energies higher than 20 eV; on the other hand, for low energies the ALDA works better, a result which agrees with intuitive expectations. The assessment of the theoretical modeling of the many-body effects is made by reducing the IXS data to a dynamical structure factor, $s(\mathbf{q}, \omega)$, defined per unit volume. Our approach has the advantage that it is applicable without modification to complex materials, such as the transition-metal oxides, which are beyond the free-electron approximation on which earlier approaches to the determination of absolute IXS cross sections relied in an essential way.

2 Theory

2.1 Time dependent density-functional theory; the linear response regime We begin by sketching the theoretical framework underlying our investigation of $S(\mathbf{q}, \omega)$, namely time-dependent density-functional theory (TDDFT) [20]. A general formulation for the problem of the time evolution of an interacting many-electron system in the presence of an external potential $v_e(\mathbf{x}, t)$ has been given by Runge and Gross [21]. These authors obtained a generalization of the Hohenberg–Kohn theorem of density-functional theory (DFT) [22] to the time-dependent domain by establishing the invertibility of the mapping $v_e(\mathbf{x}, t) \rightarrow n(\mathbf{x}, t)$, where $n(\mathbf{x}, t)$ is the time-dependent density for the actual, interacting system. From this result, and invoking non-interacting v -representability [20–23], it readily follows that $n(\mathbf{x}, t)$ may be obtained by solving the time-propagation problem for a reference single-particle system [21], i.e., the density can be calculated as

$$n(\mathbf{x}, t) = \sum_{\nu}^{\text{occupied}} |\varphi_{\nu}(\mathbf{x}, t)|^2, \quad (1)$$

in terms of the solutions $\varphi_{\nu}(\mathbf{x}, t)$ of the time-dependent Kohn–Sham equation,

$$i\hbar \frac{\partial}{\partial t} \varphi_{\nu}(\mathbf{x}, t) = \left(-\frac{\hbar^2}{2m} \nabla^2 + v_s[n](\mathbf{x}, t) \right) \varphi_{\nu}(\mathbf{x}, t), \quad (2)$$

where the single-particle potential $v_s[n](\mathbf{x}, t)$ (a functional of the time-dependent electron density) contains, in addition to the external and Hartree potentials, the exchange-correlation potential $v_{xc}[n](\mathbf{x}, t)$. Of course, as in the case of ground-state DFT, the formal simplicity of Eq. (2) results from the conceptual abstraction by which all the complications of the many-body problem have been condensed into the definition of $v_{xc}[n](\mathbf{x}, t)$. The development of realistic models for this exchange-correlation potential is thus of primary importance.

The TDDFT formalism is well suited for the study of the *linear response* of a many-electron system to a weak external potential $\delta v_e(\mathbf{x}, t)$ due to, for example, the hard X-rays used in our experimental investigations. The one-to-one mapping between $v_e(\mathbf{x}, t)$ and $n(\mathbf{x}, t)$ implies a rigorous definition of the density-response function for the interacting system,

$$\chi(\mathbf{x}t; \mathbf{x}'t') = \left. \frac{\delta n(\mathbf{x}, t)}{\delta v_e(\mathbf{x}', t')} \right|_{v_0[n_0]}, \quad (3)$$

where the functional derivative is to be evaluated at the ground-state density n_0 for the external potential $v_0(\mathbf{x})$ (due to the nuclei). Note that χ is a functional of n_0 . We also note that Eq. (3) defines, in

principle, the same density-response function encountered in more conventional many-body approaches [24].

Now the above mapping also holds in the absence of interactions; we can then introduce a single-particle, or Kohn–Sham, density-response function $\chi^{(s)}(\mathbf{x}t; \mathbf{x}'t')$ via an equation of the form of Eq. (3), but involving a derivative with respect to $v_s[n](\mathbf{x}', t')$ (the derivative is to be evaluated at $v_s[n_0]$). Making additional use of one-to-one mapping considerations (in this case, between δv_s and δv_e), and utilizing the chain rule for functional differentiation, we are led to an integral equation for the density-response function [25],

$$\chi = \chi^{(s)} + \chi^{(s)}(v + f_{xc}) \chi, \quad (4)$$

where v is the bare Coulomb interaction, and the dynamical exchange-correlation kernel f_{xc} is defined by the equation

$$f_{xc}[n_0](\mathbf{x}t; \mathbf{x}'t') = \frac{\delta v_{xc}[n](\mathbf{x}t)}{\delta n(\mathbf{x}'t')}, \quad (5)$$

where the functional derivative is to be evaluated at the ground-state density.

The spectral representation of $\chi^{(s)}$ in terms of the eigenfunctions and eigenvalues of the Kohn–Sham ground-state is of the usual form. For a periodic crystal it is convenient to work with the Fourier transform of $\chi^{(s)}$, given by the equation

$$\begin{aligned} \chi_{\mathbf{G}, \mathbf{G}'}^{(s)}(\mathbf{q}, \omega) &= \frac{1}{V} \sum_{\mathbf{k}}^{\text{BZ}} \sum_{j, j'} \frac{f_{\mathbf{k}, j} - f_{\mathbf{k}+\mathbf{q}, j'}}{E_{\mathbf{k}, j} - E_{\mathbf{k}+\mathbf{q}, j'} + \hbar(\omega + i\eta)} \langle \mathbf{k}, j | e^{-i(\mathbf{q}+\mathbf{G})\cdot\hat{\mathbf{x}}} | \mathbf{k} + \mathbf{q}, j' \rangle \\ &\times \langle \mathbf{k} + \mathbf{q}, j' | e^{i(\mathbf{q}+\mathbf{G}')\cdot\hat{\mathbf{x}}} | \mathbf{k}, j \rangle, \end{aligned} \quad (6)$$

where \mathbf{q} lies within the first Brillouin zone (BZ), \mathbf{G} is a vector of the reciprocal lattice, j is a band index, and V is the normalization volume. We evaluate Eq. (6) on the basis of Kohn–Sham states and eigenvalues obtained within the local-density approximation (LDA). In the present Fourier representation, Eq. (4) is turned into a matrix equation that we solve numerically.

The TDDFT framework embodied by Eqs. (4–6) constitutes an *exact* linear-response method for periodic solids, in which the many-body effects enter via the ground-state exchange-correlation potential $v_{xc}[n_0]$ and the many-body kernel $f_{xc}[n_0]$. All explicit effects of dynamical correlations – which, by *definition*, are beyond $v_{xc}[n_0]$ and, thus, the single-particle response $\chi_{\mathbf{G}, \mathbf{G}'}^{(s)}(\mathbf{q}, \omega)$ – are included in the many-body kernel f_{xc} . To put it graphically: Many-body effects such as self-energy shifts and lifetimes, and vertex corrections, which, in diagrammatic approaches, are built into the proper polarization function [14–26] are, in the TDDFT approach, incorporated into f_{xc} [27].

From the perspective of this article we emphasize that, when combined with measured IXS cross sections, the TDDFT linear-response scheme has, by virtue of the “partitioning” of the roles of v_{xc} and f_{xc} in the many-body problem, the potential for elucidating the dual effects of the band structure and the dynamical many-body correlations – a theme which is very topical in many areas of contemporary condensed-matter physics. This is possible, for example, whenever an LDA description of the band structure is representative of the result expected from the exact v_{xc} . In that case, the Kohn–Sham response $\chi^{(s)}$ can be considered to be “sufficiently close” to its exact value; thus, eventual deviations between theory and the measured cross sections are attributable to the role of the dynamical correlations built into f_{xc} . The case of Al discussed below represents a realization of this scenario.

2.2 The dynamical structure factor We recall the result for the double differential scattering cross-section within the (first) Born approximation:

$$\frac{d^2\sigma}{d\Omega d\omega} = \left(\frac{d\sigma}{d\Omega} \right)_0 S(\mathbf{q}, \omega), \quad (7)$$

where, in the case of inelastic X-ray scattering (IXS), we have that

$$\left(\frac{d\sigma}{d\Omega}\right)_0 = r_0^2 (\mathbf{e}_i \cdot \mathbf{e}_f)^2 \left(\frac{\omega_f}{\omega_i}\right), \quad (8)$$

where $r_0 = e^2/mc^2$ is the “classical electron radius,” and the remaining variables refer to the polarization vector and frequency of the incident (“*i*”) and scattered (“*f*”) photons.

For a periodic crystal, the fluctuation-dissipation theorem translates into the (exact) result that (for $T = 0$ K)

$$S(\mathbf{q}, \omega) = -2\hbar V \operatorname{Im} \chi_{G,G}(\mathbf{q} - \mathbf{G}, \omega), \quad (9)$$

where V is, as in Eq. (6), the volume of the macrocrystal on whose sides we apply periodic boundary conditions. Clearly, $S(\mathbf{q}, \omega)$ is an extensive quantity. Now, in practice the thermodynamic limit is only realized for sufficiently large volumes; in that case, any residual (numerical) dependence of $\operatorname{Im} \chi_{G,G}(\mathbf{q} - \mathbf{G}, \omega)$ on V is gone, and the only such dependence in Eq. (9) is via the overall factor of the volume V ; this can be checked via calculations for denser and denser wave-vector meshes – which define a new V in each case.

We can then (i.e., for sufficiently dense k -meshes) define a dynamical structure factor per unit volume, $s(\mathbf{q}, \omega)$, by pulling the factor V from the above result, i.e.,

$$s(\mathbf{q}, \omega) = \frac{1}{V} S(\mathbf{q}, \omega) = -2\hbar \operatorname{Im} \chi_{GG}(\mathbf{q} - \mathbf{G}, \omega), \quad (10)$$

and define a scattering cross section per unit volume,

$$\frac{1}{V} \frac{d^2\sigma}{d\Omega d\omega} = \left(\frac{d\sigma}{d\Omega}\right)_0 s(\mathbf{q}, \omega). \quad (11)$$

We stress that in Eqs. (10) and (11) there are no arbitrary multiplicative constants. The left hand side represents a quantity experimentally measurable in absolute units – *e.g.*, via the procedure we outline below – independently of the atomic structure of the material, or of any assumption about the nature of the electrons (valence, semi-core, etc.) that may participate in the excitation process. This point is crucial for a meaningful assessment of the relative roles of band structure and dynamical correlations. Although it is common practice to present dynamical structure factors obtained via IXS and inelastic neutron scattering in terms of structural units such as atoms or primitive unit cells, the explicit determination of $s(\mathbf{q}, \omega)$ in the “natural” units of Eq. (10) (*e.g.*, $\text{eV}^{-1} \text{\AA}^{-3}$, as in Figs. (2–4)), rather than structural units specific to a particular material, produces data with no ambiguity – even for complex materials in which free-electron-gas descriptions (and a related “tagging” of the electrons that participate in the dynamical response) are out of the question.

3 Experiment Inelastic X-ray scattering measurements on Al have been made on the X-21 beamline at the National Synchrotron Light Source (NSLS) with an energy resolution 0.75 eV using a four-crystal monochromator and on the UNI-CAT beamline at the Advanced Photon Source (APS) with an energy resolution of 1.1 eV provided by the two-crystal high heat load monochromator as illustrated in Fig. 1. The X-21 wiggler beamline produced a 10 keV incident X-ray beam with a power of $\sim 10^{10}$ Hz onto an area of $0.75 \times 1 \text{ mm}^2$. The sagittal focusing Si (111) monochromator on the UNI-CAT undulator beamline provided a $\sim 0.1 \times 0.25 \text{ mm}^2$ beam at 7.5 keV with $\sim 2 \times 10^{12}$ Hz on the sample. The scattered beam energy analyses were performed by spherically bent, ~ 40 mm diameter Ge and Si analyzers located in back-reflection geometry 1 m from the sample at the APS and NSLS, respectively. Low noise avalanche photodiode X-ray detectors located 1 m from the analyzer at scattering angles of $> 176^\circ$.

The measurements were performed on $\langle 001 \rangle$ and $\langle 013 \rangle$ oriented aluminum single crystals oriented in the symmetric Bragg geometry as depicted in Fig. 1. Relative $s(\mathbf{q}, \omega)$ measurements made on the X-21 beamline at the NSLS for wave vectors of 1.0, 1.5, 1.7, and 2.0 k_F along the [013] direction and

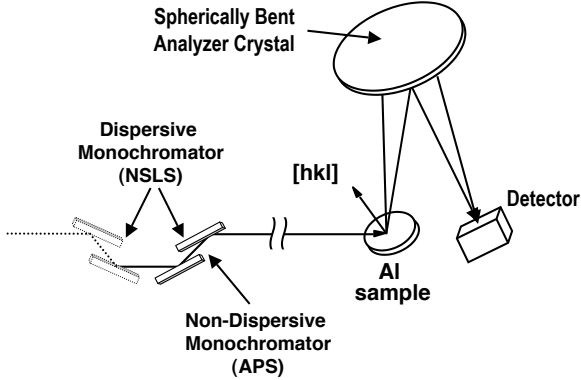


Fig. 1 Schematic view of the inelastic scattering geometry used for measurements on the NSLS X-21 beam line (four-bounce monochromator) and on the APS ID-33 UNI-CAT beamline (2-bounce monochromator). A Si (555) analyzer was used for the NSLS measurements and a Ge (444) analyzer was used at the APS.

at $1k_F$ along the [001] direction were reduced to absolute units by scaling the $1k_F$ [001] NSLS measurements to match the absolute $s(\mathbf{q}, \omega)$ measurements made at the APS at a wave vector $1k_F$ in the [001] direction of Al.

The APS data were reduced to absolute units using the first moment f sum-rule relationship given by

$$\int_0^{\infty} s(\mathbf{q}, \hbar\omega) (\hbar\omega) d(\hbar\omega) = \pi n(\mathbf{G} = 0) \frac{(hc)^2}{mc^2} \left(\frac{q}{2\pi}\right)^2 \left[\frac{\text{eV}}{\text{\AA}^3}\right], \quad (12)$$

where $n(\mathbf{G} = 0) = N/V$ is the average electron density (here N is the number of electrons contributing to this sum rule).

For measurements that do not extend past the Al L-edge (72 eV), only the three valence electrons contribute to the sum rule. In principle, this represents a straightforward technique for calibration of the efficiency of the geometry and energy analysis system; however, it is complicated by the fact that crystal local-field effects extend the cutoff energy of the inelastic scattering to energies significantly beyond the ~ 35 eV jellium cutoff and beyond the 72 eV semi-core onset energy (i.e. L-edge), as seen in the measurements in Fig. 2; these measurements were performed on the UNI-CAT ID-33 beamline at the Advanced Photon Source. We have used pseudopotential based $s(\mathbf{q}, \omega)$ calculations to estimate the ratio of the contribution to the f sum-rule for energies greater than and less than 65 eV for Al at $1k_F$. It was found that 95% of the first moment is fulfilled by 65 eV. As described previously [15, 28], the first principles calculations were made using Troulier–Martins non-local, norm-conserving, pseudopotentials with a cutoff of 12 Ryd. The data for all wave-vectors and all orientations measured at

the X-21 beamline at NSLS were reduced to absolute units by scaling X-21 measurements at $1k_F$ in the [001] direction to the intensity profile in Fig. 2 between ~ 10 –35 eV. This avoided the requirement of measuring the low intensity tails of the loss spectrum with the lower beam powers available at the NSLS.

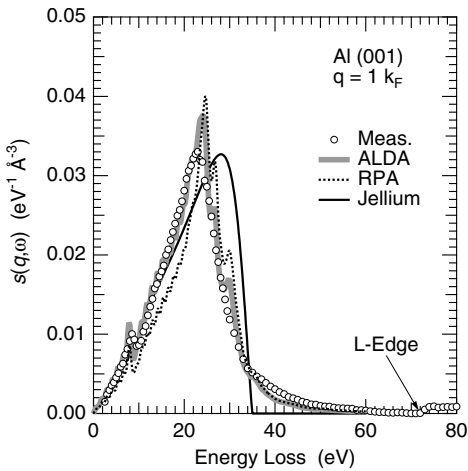


Fig. 2 Absolute IXS measurements (circles) made on Al at the UNI-CAT beamline at the APS together with $s(\mathbf{q}, \omega)$ calculations for Jellium (thin dark line), RPA (dotted line), and LDA (thick gray line).

Transition metals and insulators do not provide the possibility of direct f sum-rule scaling such as described for Al. However, since the scaling of energy loss spectrum measurements in units of $\text{eV}^{-1} \text{\AA}^{-3}$ depends only on the effective volume of material sampled by the X-ray beam, it is possible to transfer the calibration factor for absolute $s(\mathbf{q}, \omega)$ measurements made on an Al crystal to $s(\mathbf{q}, \omega)$ measurements on an arbitrary sample, X , simply by accounting for the difference in the sample volumes probed. For thick samples and symmetric Bragg geometry, the volume ratio is given by the ratio of the linear absorption coefficients, $\mu(X)/\mu(\text{Al})$. That is, scaling relative $I(\mathbf{q}, \omega)/I_0$ measurements (I_0 is the incident beam power) on Al at $1k_F$ by a factor, C , to the profile in Fig. 2, yields absolute $s_{\text{Al}}(\mathbf{q}, \omega) = CI_{\text{Al}}(\mathbf{q}, \omega)/I_0$ for Al. Then, relative $I_X(\mathbf{q}, \omega)/I_0$ measurements performed on material X in symmetric Bragg geometry can be reduced to absolute $s_X(\mathbf{q}, \omega)$ measurements through

$$s_X(\mathbf{q}, \omega) = \frac{V_{\text{Al}}}{V_X} C \frac{I_X(\mathbf{q}, \omega)}{I_0} = \frac{\mu_X}{\mu_{\text{Al}}} C \frac{I_X(\mathbf{q}, \omega)}{I_0} \quad (13)$$

and similar considerations apply for transmission or non-symmetric scattering geometries. Although independent tests of the calibration have not been made, we believe this technique provides an absolute scaling with an accuracy of $\sim 5\text{--}10\%$. The main limitation to the accuracy is proper specification of the background scattering under the inelastic loss spectrum for the standard Al sample. Although the uncertainties in this background are small, errors in this value are magnified by the first moment over the wide energy range.

4 Results Inelastic X-ray scattering measurements of $s(\mathbf{q}, \omega)$ made on aluminum at the X-21 beamline at the NSLS are plotted in absolute units of $\text{eV}^{-1} \text{\AA}^{-3}$ in Figs. 3 and 4 for wave vectors $q = 1.75, 2.625, 2.975$ and 3.5\AA^{-1} directed along the [013] direction. Measurements along the [013] direction (rather than, say, the higher symmetry [001] direction) avoid the complication of the (002) Bragg reflection at $1.77k_F$ and minimize band-structure-related modulations in the loss spectrum. In units of the Fermi wave vector ($k_F = 1.75 \text{\AA}^{-1}$ for Al) these wave vector transfers correspond to 1.0, 1.5, 1.7, and $2.0 k_F$, all of which are well above the $0.65k_F$ onset of Landau damping (with reference to the standard value for jellium). The measurements show the broadening of the loss spectrum with increasing wave vector characteristic of nearly free electron materials, and they show the band-structure induced dip in the spectrum at ~ 30 eV that attracted both experimental and theoretical interest over the years [12–15].

Also plotted in Figs. 3 and 4 are $s(\mathbf{q}, \omega)$ spectra calculated within the TDDFT framework outlined above [14]. In addition to the ALDA, we present results obtained in the random-phase approximation (RPA), which corresponds to setting $f_{xc} = 0$ (note that the LDA band structure is embedded in the Kohn–Sham response function). We also consider the spectra obtained with use of the explicitly frequency-dependent, complex, f_{xc} obtained by Devreese, Brosens, and Lemmens [3], and by Brosens, Devreese, and Lemmens (BDL) [6] for an electron gas via a dynamical-exchange decoupling procedure (equivalent to time-dependent Hartree–Fock), in which the Coulomb “ladders” are bare, i.e., unscreened.

We note that both the ALDA and BDL kernels lead to a good overall description of the energy loss spectrum for $1.0k_F$. For $1.5k_F$, the BDL f_{xc} tends to overestimate the energy loss somewhat for low frequencies while the LDA f_{xc} provides a rather good description of the spectrum below 20 eV. Neither the BDL nor the LDA kernels provide a full account of the measurements for frequencies above 30 eV. As shown in Fig. 4, for the larger wave vectors of 1.7 and $2k_F$, the ALDA continues to provide reasonable agreement with the measured spectra. Although the use of the BDL f_{xc} yields an excess weight below ~ 10 eV, for higher frequencies it seems to provide somewhat better agreement with the data than the ALDA, as exemplified for $1.7k_F$.

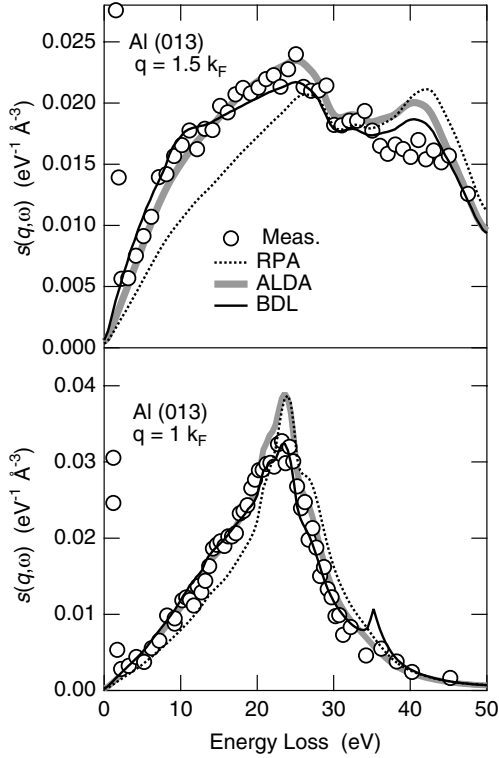


Fig. 3 Absolute IXS measurements (circles) made on Al for a wave vectors of 1.0 and $1.5k_F$ on the X-21 beamline at the NLS together with TDDFT $s(\mathbf{q}, \omega)$ calculations for RPA (dotted line), LDA (thick gray line), and BDL (thin dark line).

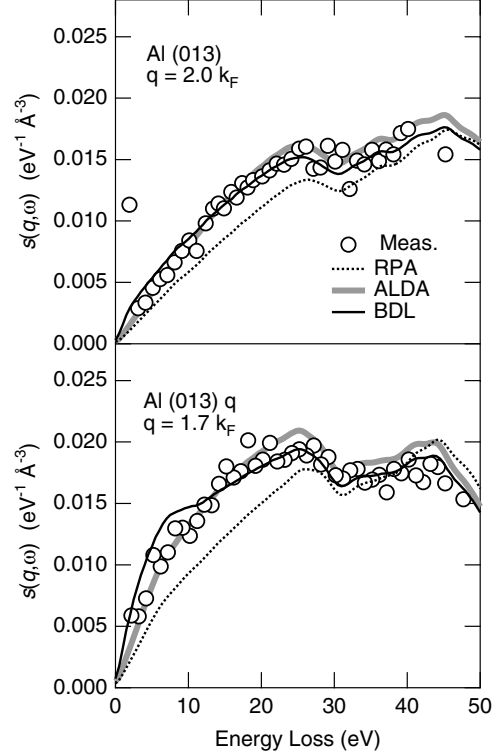


Fig. 4 Absolute IXS measurements (circles) made on Al for a wave vectors of 1.7 and $2.0k_F$ on the X-21 beamline at the NLS together with TDDFT $s(\mathbf{q}, \omega)$ calculations for RPA (dotted line), LDA (thick gray line), and BDL (thin dark line).

5 Discussion The results shown in Figs. 3 and 4 indicate that the ALDA provides a good overall description of the Al energy loss spectrum in the [013] direction for q -values up to $2k_F$ and frequencies up to ~ 20 eV. This is in contrast to our earlier report of significant discrepancies between the ALDA and the IXS data for Al [15]. Such large discrepancies are not found in these new measurements made using the more reliable spherically bent energy analyzer geometry (see Fig. 1). The problem with the early measurements has not been determined completely yet; we believe that this issue is associated with a systematic error in calibrating the inhomogeneous mosaic-spread in the pyrolytic graphite energy analyzer used in the earlier measurements [15]. The spherically-bent energy analyzer geometry used here and in Ref. [28] avoids such issues.

Comparing the loss-spectra obtained with the BDL and ALDA kernels, we note in general that the BDL result tends to be in reasonably good agreement with measured data for frequencies above ~ 15 eV. On the other hand, the BDL kernel systematically overestimates the spectral weight for frequencies below ~ 15 eV for all wave vectors. Bearing in mind that the BDL kernel includes dynamical exchange but does not include correlations, it does not seem surprising that better agreement is achieved at larger frequencies for which correlations are expected to be less important.

It is useful to point out that the nearly rigid offset between $s(\mathbf{q}, \omega)$ obtained with ALDA and BDL kernels for wave vectors of 1.7 and $2k_F$ (and frequencies above ~ 20 eV) is traceable largely to the imaginary part of the BDL f_{xc} . To the extent that the offset puts the BDL result in slightly better agreement with the measured data for these higher frequencies, this result underscores the importance in general of the inclusion of dynamic effects.

Although consideration of additional f_{xc} formulations is beyond the scope of this article, it will of course be of interest to consider the results for $s(\mathbf{q}, \omega)$ obtained with use of other kernels in the literature, such as the one obtained by Richardson and Ashcroft [4]. That kernel incorporates both exchange and correlations in a dynamic f_{xc} . We believe that direct comparison of *ab initio* TDDFT calculations of $s(\mathbf{q}, \omega)$ (based on well defined f_{xc} kernels) with absolute IXS measurements of $s(\mathbf{q}, \omega)$ (over wide frequency and wave vector ranges) provides both a stringent test of f_{xc} kernels and a straightforward procedure for the investigation of electronic correlations in both simple and complex materials. In case the LDA description of the static V_{xc} kernel is not suitable for complex materials, IXS data would provide tests for non-trivial “models” of V_{xc} and f_{xc} .

6 Conclusion The direct connection between inelastic X-ray scattering measurements and time-dependent density functional theory calculations has been exploited to investigate short-range electronic correlations in Al. A procedure capable of extending absolute IXS measurements to complex electronic systems such as transition metals and transition-metal oxides has been presented. Comparison of the frequency and wave vector dependence of *ab initio* calculations of $s(\mathbf{q}, \omega)$ for Al with IXS measurements have shown that the ALDA provides a good overall account of the energy loss spectra for wave vectors up to $2k_F$, contrary to the conclusions of a previous report [15]. Use of the BDL kernel was shown to provide a good match to experiment for large frequencies, but not for low frequencies where correlations are expected to be more important. Our work suggests that a combination of high-precision IXS measurements with state-of-the-art TDDFT calculations for periodic crystals offers a promising framework for benchmark-development towards the goal of fundamental treatments of dynamical correlations in real materials.

Acknowledgments We thank C.-C. Kao for help on the NSLS X-21 beamline and advice and discussions during this work. This research was sponsored in part (A.G.E.) through NSF Grant ITR DMR-0219332 and in part by the US Department of Energy, Basic Energy Sciences, Division of Materials Sciences under contract DE-AC05-00OR22725 with Oak Ridge National Laboratory, managed by UT-Battelle, LLC. UNICAT is supported by the Univ. of IL-MRL, Oak Ridge National Lab., National Institute for Standards and Technology, and UOP, Inc. Use of the UNICAT beamline at the Advanced Photon Source and the X-21 beamline at the NSLS was supported by the U.S. Department of Energy, Office of Science, Office of Basic Energy Sciences.

References

- [1] J. C. Kimball, Phys. Rev. A **7**, 1648 (1973).
- [2] P. Vashishta and K. S. Singwi, Phys. Rev. B **6**, 875 (1972).
- [3] J. T. Devreese, F. Brosens, and L. F. Lemmens, Phys. Rev. B **21**, 1349 (1980).
- [4] C. F. Richardson and N. W. Ashcroft, Phys. Rev. B **50**, 8170 (1994).
- [5] S. Moroni, D. M. Ceperley, and G. Senatore, Phys. Rev. Lett. **75**, 689 (1995).
- [6] F. Brosens, J. T. Devreese, and L. F. Lemmens, Phys. Rev. B **21**, 1363 (1980).
- [7] Y.-H. Kim and A. Görling, Phys. Rev. Lett. **89**, 096402 (2002).
- [8] L. Reining, V. Olevano, A. Rubio, and G. Onida, Phys. Rev. Lett. **88**, 066404 (2002).
- [9] I. V. Tokatly and O. Pankratov, Phys. Rev. Lett. **86**, 2078 (2001).
- [10] X. Gonze and M. Scheffler, Phys. Rev. Lett. **82**, 4416 (1999).
- [11] W. Schülke and U. Berg, phys. stat. sol. **23**, K87 (1967).
- [12] W. Schülke, H. Nagasawa, S. Mourikis, and A. Kaprolat, Phys. Rev. B **40**, 12215 (1989).
- [13] P. M. Platzman, E. D. Isaacs, H. Williams, P. Zschack, and G. E. Ice, Phys. Rev. B **46**, 12943 (1992).
- [14] A. Fleszar, A. A. Quong, and A. G. Eguiluz, Phys. Rev. Lett. **74**, 590 (1995).
- [15] B. C. Larson, J. Z. Tischler, E. D. Isaacs, P. Zschack, A. Fleszar, and E. G. Eguiluz, Phys. Rev. Lett. **77**, 1346 (1996).
- [16] J. P. Hill, C.-C. Kao, W. A. C. Caliebe, D. Gibbs, and J. B. Hastings, Phys. Rev. Lett. **77**, 3665 (1996).
- [17] W. Schülke, J. R. Schmitz, H. Schulte-Schrepping, and A. Kaprolat, Phys. Rev. B **52**, 11721 (1995).
- [18] A. G. Eguiluz, W. Ku, and J. M. Sullivan, J. Chem. Phys. Solids **61**, 383 (2000).
- [19] G. Onida, L. Reining, and A. Rubio, Rev. Mod. Phys. **74**, 601 (2002).
- [20] For a timely, insightful review of the foundations and practical implementations of TDDFT, see N. T. Maitra, K. Burke, H. Appel, E. K. U. Gross, and R. van Leeuwen, in Reviews in Modern Quantum Chemistry:

- A Celebration of the Contributions of R. G. Parr, edited by K. D. Sen (World Scientific, Singapore, 2002). See also K. Burke and E. K. U. Gross, in *Density Functionals: Theory and Applications*, edited by D. Joubert (Springer, Berlin, 1998), p. 116.
- [21] E. Runge and E. K. U. Gross, *Phys. Rev. Lett.* **52**, 2850 (1984).
 - [22] P. Hohenberg and W. Kohn, *Phys. Rev.* **136**, B864 (1964);
W. Kohn and L. J. Sham, *Phys. Rev.* **140**, A1133 (1965).
 - [23] R. van Leeuwen, *Phys. Rev. Lett.* **82**, 3863 (1999); *Int. J. Mod. Phys. B* **15**, 1969 (2001).
 - [24] G. D. Mahan, *Many Particle Physics*, 2nd ed. (Plenum, New York, 1990), Chapter 5.
 - [25] M. Petersilka, U. J. Gossmann, and E. K. U. Gross, *Phys. Rev. Lett.* **76**, 1212 (1996).
 - [26] A. G. Eguiluz and W. Ku, in *Electron Correlations and Materials Properties*, edited by A. Gonis, N. Kioussis, and M. Ciftan (Kluwer-Plenum, N.Y., 1999), p. 329.
 - [27] In particular, we stress that “self-energy shifts” should not be introduced in the Kohn–Sham response – even if that procedure were to yield apparent agreement with the data. Unfortunately, such uncontrolled approximation, particularly involving GW self-energy shifts, has become rather common in the literature.
 - [28] B. C. Larson, J. Z. Tischler, A. Fleszar, and A. G. Eguiluz, *J. Phys. Chem. Solids* **61**, 391 (2000).